Nuclear fusion in dense matter: Reaction rate and carbon burning

L. R. Gasques,[1] A. V. Afanasjev,[1] E. F. Aguilera,[2] M. Beard,[1] L. C. Chamon,[3] P. Ring,[4] M. Wiescher,[1] and D. G. Yakovlev[5]

[1]*Department of Physics & The Joint Institute for Nuclear Astrophysics, University of Notre Dame, Notre Dame, Indiana 46556 USA*
[2]*Departamento del Accelerador, Instituto Nacional de Investigaciones Nucleares, A.P. 18-1027, C.P. 11801, Destrito Federal, Mexico*
[3]*Departamento de Física Nuclear, Instituto de Física da Universidade de São Paulo, Caixa Postal 66318, 05315-970, São Paulo, SP, Brazil*
[4]*Physik-Department, Technische Universitat München, D-85747, Garching, Germany*
[5]*Ioffe Physical Technical Institute, Poliekhnicheskaya 26, RU-194021 St. Petersburg, Russia*

In this paper we analyze the nuclear fusion rates among equal nuclei for all five different nuclear burning regimes in dense matter (two thermonuclear regimes, two pycnonuclear ones, and the intermediate regime). The rate is determined by Coulomb barrier penetration in dense environments and by the astrophysical S factor at low energies. We evaluate previous studies of the Coulomb barrier problem and propose a simple phenomenological formula for the reaction rate that covers all cases. The parameters of this formula can be varied to take into account current theoretical uncertainties in the reaction rate. The results are illustrated for the example of the $^{12}C+^{12}C$ fusion reaction. This reaction is important for the understanding of nuclear burning in evolved stars, in exploding white dwarfs producing type Ia supernovas, and in accreting neutron stars. The S factor at stellar energies depends on a reliable fit and extrapolation of the experimental data. We calculate the energy dependence of the S factor by using a recently developed parameter-free model for the nuclear interaction, taking into account the effects of the Pauli nonlocality. For illustration, we analyze the efficiency of carbon burning in a wide range of densities and temperatures of stellar matter with the emphasis on carbon ignition at densities $\rho \gtrsim 10^9$ g cm^{-3}.

I. INTRODUCTION

We study nuclear fusion rates of identical nuclei in dense stellar matter. This problem is of utmost importance for understanding the structure and evolution of stars of various types. Despite the efforts of many authors, the theoretical reaction rates are still rather uncertain, especially at high densities. The uncertainties have two aspects. The first one is related to *nuclear physics* and is concerned with the proper treatment of *nuclear* interaction transitions (conveniently described in terms of the astrophysical factor S). The other issue is associated with aspects of *plasma physics* and concerns the proper description of Coulomb barrier penetration (BP) in a high-density many-body system. We analyze both aspects and illustrate the results, taking the carbon fusion reaction as an example.

Considerable experimental effort has been expended on the study of low-energy fusion reactions such as $^{12}C+^{12}C$ to investigate the impact on the nucleosynthesis, energy production, and time scale of late stellar evolution. Nevertheless, it has been difficult to develop a global and reliable reaction formalism to extrapolate the energy dependence of the fusion cross section into the stellar energy range. The overall energy dependence of the cross section is determined by the Coulomb barrier tunnel probability. One goal of the present work is to apply the São Paulo potential model to provide a general description of the stellar fusion processes. This model does not contain any free parameters and represents a powerful tool for predicting average low-energy cross sections for a wide range of fusion reactions, as long as the density distribution of the nuclei involved in the reaction can be determined. In this context we also seek to introduce a phenomenological formalism for a generalized reaction rate to describe all the regimes of

nuclear burning in a one-component plasma ion system. In this paper we want to demonstrate the applicability of the method on the specific example of $^{12}C+^{12}C$ and to evaluate the reliability and uncertainty range of the proposed formalism through the comparison with the available low-energy data. In a subsequent publication we want to extend the model to multi-ion systems with the aim of simulating a broad range of heavy-ion nucleosynthesis cases, from thermonuclear burning in hot stellar plasma to pycnonuclear burning in high-density crystalline stellar matter.

Carbon burning represents the third phase of stellar evolution for massive stars ($M \gtrsim 8M_{\odot}$); it follows helium burning that converts He fuel to ^{12}C by means of the triple α process. Carbon burning represents the first stage during stellar evolution determined by heavy-ion fusion processes (e.g., Ref. [1]). The most important reaction during the carbon burning phase is the $^{12}C+^{12}C$ fusion [2]; additional processes can be $^{12}C+^{16}O$ and $^{16}O+^{16}O$, depending on the $^{12}C/^{16}O$ abundance ratio, which is determined by the $^{12}C(\alpha,\gamma)^{16}O$ reaction rate [3,4]. The most important reaction branches are $^{12}C(^{12}C,\alpha)^{20}Ne$ ($Q = 4.617$ MeV) and $^{12}C(^{12}C,p)^{23}Na$ ($Q = 2.241$ MeV). Carbon burning in evolved massive stars takes place at typical densities of $\rho \sim 10^5$ g cm^{-3} and temperatures $T \sim (6-8) \times 10^8$ K.

Carbon burning is also crucial for type Ia supernovas. These supernova explosions are driven by carbon ignition in cores of accreting massive CO white dwarfs [5]. The burning process proceeds from the carbon ignition region near the center of a white dwarf by detonation or deflagration through the entire white dwarf body. The ignition conditions and time scale are defined by the $^{12}C+^{12}C$ reaction rate, typically at $T \sim (1.5-7) \times 10^8$ K and $\rho \sim (2-5) \times 10^9$ g cm^{-3} [6,7].

Depending on the ^{16}O abundance, other fusion reactions may also contribute. For these high densities the reaction cross sections are affected by strong plasma screening, which reduces the repulsive Coulomb barrier between interacting ^{12}C or ^{16}O nuclei (e.g., Refs. [8,9]; also see Sec. III).

Explosive carbon burning in the crust of accreting neutron stars has recently been proposed as a possible trigger and energy source for superbursts [10–12]. In this case, small amounts of carbon (3–10%), which have survived in the preceding rp-process phase during the thermonuclear runaway, ignite after the rp-process ashes are compressed by accretion to a density of $\rho \sim 1.3 \times 10^9$ g cm^{-3}. The ignition of a carbon flash requires an initial temperature of $T \gtrsim 10^9$ K, triggering a photodisintegration runaway of the rp-process ashes after a critical temperature of $T \sim 2 \times 10^9$ K is reached [13]. For these cases, carbon burning proceeds in the *thermonuclear* regime with strong plasma screening (see Sec. III for details).

At high densities and/or low temperatures the thermonuclear reaction-rate formalism is insufficient because the fusion process is mainly driven by the high-density conditions in stellar matter (Secs. III and IV). This is particularly important for nuclear fusion in the deeper layers of the crust of an accreting neutron star [14]. At sufficiently high ρ and low T, nuclei form a crystalline lattice. Neighboring nuclei may penetrate the Coulomb barrier and fuse owing to zero-point vibrations in their lattice sites. In this *pycnonuclear* burning regime the reaction rate depends mainly on the density and is nearly independent of temperature (e.g. [15,16]). Pycnonuclear burning regimes may not be limited to carbon-induced fusion reactions only, but may be driven by a broad range of fusion reactions between stable and neutron-rich isotopes [14].

In Sec. II, we discuss the theory of fusion cross sections and calculate the astrophysical S factor for carbon burning in the framework of a generalized parameter-free potential model. In Sec. III we study the Coulomb barrier problem for identical nuclei, and propose an expression for the reaction rate that describes all the regimes of nuclear burning in a dense one-component plasma of atomic nuclei. In Sec. IV we analyze, for illustration, the main features of ^{12}C burning from high-temperature gaseous or liquid plasma to high-density crystalline matter. We summarize and conclude in Sec. V.

II. FUSION CROSS SECTION AND ASTROPHYSICAL S FACTOR

Nuclear reactions are possible after colliding nuclei tunnel through the Coulomb barrier. Recently, a parameter-free model for the real part of the nuclear interaction (São Paulo potential) based on nonlocal quantum effects was developed [17–20]. In previous work [21], this model was applied to the study of fusion processes by use of the BP formalism for about 2500 cross-section data, corresponding to approximately 165 different systems. Within the nonlocal model, the bare interaction $V_N(r, E)$ is connected with the folding potential $V_F(r)$:

$$V_N(r, E) = V_F(r)e^{-4v^2/c^2}, \quad (1)$$

where c is the speed of light, E is the particle collision energy (in the center-of-mass reference frame), v is the local relative velocity of the two nuclei 1 and 2,

$$v^2(r, E) = \frac{2}{\mu}\left[E - V_C(r) - V_N(r, E)\right], \quad (2)$$

$V_C(r)$ is the Coulomb potential, $\mu = A_1 A_2 m_u/(A_1 + A_2)$ is the reduced mass, and m_u is the atomic mass unit. The folding potential depends on the matter densities of the nuclei involved in the collision:

$$V_F(R) = \int \rho_1(\boldsymbol{r}_1)\, \rho_2(\boldsymbol{r}_2)\, V_0\, \delta(\boldsymbol{R} - \boldsymbol{r}_1 + \boldsymbol{r}_2)\, d\boldsymbol{r}_1, \quad (3)$$

with $V_0 = -456$ MeV fm^3. The use of the matter densities and delta function in Eq. (3) corresponds to the zero-range approach for the folding potential, which is equivalent [20] to the more usual procedure of using the M3Y effective nucleon-nucleon interaction with the nucleon densities of the nuclei. The advantage in adopting the São Paulo potential to describe the fusion cross section relies on the fact that no additional parameter is necessary once the density distribution of the participating nuclei has been determined. The model is therefore a good choice for a generalized treatment of low-energy heavy-ion fusion reactions.

There are several ways to determine the nuclear density distribution [20,22–28]. Density functional theories (DFTs) provide for example a successful description of many nuclear ground-state properties, in particular, of charge distributions in the experimentally known region. Because these theories are universal in the sense that their parameter sets are carefully adjusted and valid all over the periodic table, one can expect that they also yield reliable predictions for nuclei far from stability. Nonrelativistic density functionals, such as the Skyrme or Gogny functional, have been widely used in the literature. In recent years, relativistic density functionals have played an increasingly important role because they provide a fully consistent description of the spin-orbit splitting. This is of greatest importance for nuclei far from stability. The spin-orbit splitting determines the shell structure, the most basic ingredient in any microscopic theory of finite nuclei. In fact, the results obtained with relativistic functionals are in very good agreement with experimental data, throughout the periodic table, despite having a smaller number of adjustable parameters in comparison with the nonrelativistic case. Best known is the relativistic Hartree-Bogoliubov (RHB) theory [22–24], which includes pairing correlations with finite-range pairing forces. It provides a unified description of mean-field and pairing correlations in nuclei.

These functionals contain a strong density dependence, either through nonlinear coupling terms between the meson fields (e.g., in the Lagrangians with the parameter sets NL2 [25] and NL3 [26]) or by use of an explicit density dependence for the meson-nucleon vertices (e.g., in the parameter sets DD-ME1 [27] and DD-ME2 [28]).

In this paper, we consider only spherical nuclear shapes. Pairing correlations are in principle included, but they vanish for the ^{12}C nucleus. In Fig. 1 we compare the calculated densities with experimental data [29]. The RHB calculations
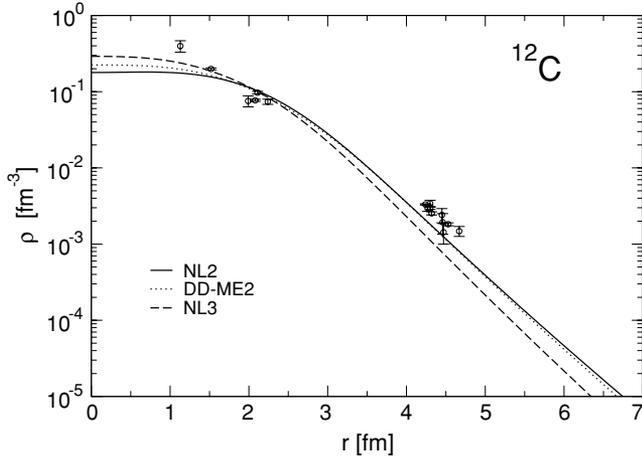
FIG. 1. Self-consistent densities for the ground state of ^{12}C calculated with different parametrizations of the relativistic mean field (RMF) Lagrangian. The densities obtained with the DD-ME1 and DD-ME2 interactions are very similar. The experimental data are taken from Ref. [29].

are in good agreement with surface properties best described by the NL2, DD-ME1, and DD-ME2 effective interactions.

To apply the BP model for calculating fusion cross sections, one needs the effective potential defined as a sum of the Coulomb, nuclear, and centrifugal components:

$$V_{\text{eff}}(r, E) = V_C(r) + V_N(r, E) + \frac{\ell(\ell + 1)\hbar^2}{2\mu r^2}. \qquad (4)$$

Following the BP model, one can associate the fusion cross section with the particle flux transmitted through the barrier:

$$\sigma_{ij}(E) = \frac{\pi}{k^2} \sum_{\ell=0}^{\ell_{\text{cr}}} (2\ell + 1) \, T_\ell. \qquad (5)$$

It is important to point out that the sum in Eq. (5) is performed up to a maximum ℓ wave (ℓ_{cr}), which corresponds to the greatest value of angular momentum that produces a pocket (and a barrier) in the corresponding effective potential, Eq. (4). For ℓ waves with effective barrier heights $V_{B\ell} < E$, the shape of the effective potential can be approximated by a parabola with curvature defined as

$$\hbar\omega_\ell = \left| \frac{\hbar^2}{\mu} \frac{d^2 V_{\text{eff}}}{dr^2} \right|_{R_{B\ell}}^{1/2}, \qquad (6)$$

where $R_{B\ell}$ is the barrier radius. In such cases, the transmission coefficients have been obtained through the Hill-Wheeler formula [30]:

$$T_\ell = \left\{ 1 + \exp\left[\frac{2\pi(V_{B\ell} - E)}{\hbar\omega_\ell} \right] \right\}^{-1}. \qquad (7)$$

On the other hand, for ℓ waves with $V_{B\ell} > E$, we employ, instead of the Hill-Wheeler formula, a more appropriate heuristic treatment based on a WKB approximation [31]:

$$T_\ell = [1 + \exp(S_\ell)]^{-1}, \qquad (8)$$

$$S_\ell = \int_{r_1}^{r_2} \sqrt{\frac{8\mu}{\hbar^2}[V_{\text{eff}}(r, E) - E]} \, dr, \qquad (9)$$
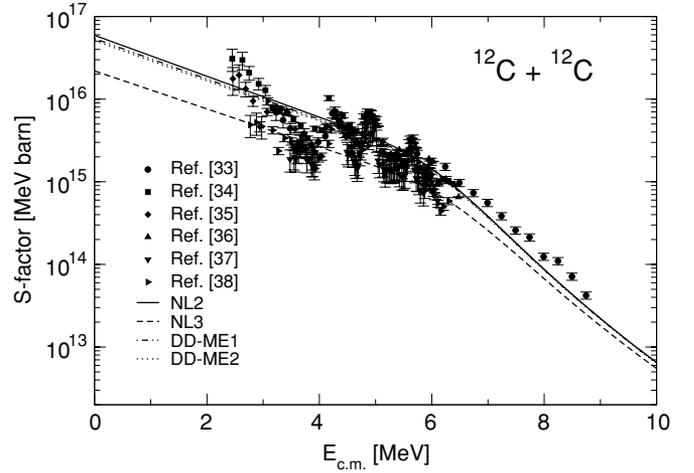
FIG. 2. Astrophysical factor $S(E)$ as a function of the center-of-mass energy E, derived from experimentally measured cross sections. Curves show theoretical results obtained within the BP model for the different model density distributions (see text for details). Various symbols denote experimental results.

where r_1 and r_2 are the classical turning points. At low energies, the WKB method gives values for the transmission coefficients that are quite different from those of the Hill-Wheeler formula. In this case, we define the barrier curvature by connecting Eqs. (6) and (7):

$$\hbar\omega_\ell = \frac{2\pi(V_{B\ell} - E)}{S_\ell}. \qquad (10)$$

The overall results provided by the BP model are in very good agreement with the fusion data for energies above the s-wave barrier height. For light systems ($\mu \leqslant 8m_u$) the model also shows very good agreement with fusion data at subbarrier energies [21]. Therefore the use of the BP model in calculating the fusion cross section at energies of astrophysical interest for the ^{12}C+^{12}C system is entirely justified.

Historically, reaction cross sections $\sigma(E)$ at very low energies, typical for astrophysical conditions, have been expressed in terms of the astrophysical S factor (e.g., Ref. [32]):

$$S(E) = \sigma(E)E \, e^{2\pi\eta}, \qquad (11)$$

where $\eta = (Z_1 Z_2 e^2/\hbar)\sqrt{\mu/(2E)}$ is the usual Gamow parameter.

Considerable efforts have been made over the past decades to measure the ^{12}C+^{12}C fusion cross section at very low energies [33–38]. The experimentally determined S factors are shown in Fig. 2. For reaction-rate calculations the experimental S-factor needs to be extrapolated toward the stellar energy range, the Gamow window, which depends sensitively on the temperature and density conditions of the stellar environment. The typical range of energy E for thermonuclear carbon burning, in the center-of-mass reference, varies from 1 to 4 MeV. For pycnonuclear carbon burning in the neutron star crusts, the energies can be as low as 10 keV. Large discrepancies between the different experimental results at low energies complicate a reliable extrapolation of $S(E)$ toward such low E. In addition, the S factor shows pronounced resonant structures, presumably

resulting from quasi-molecular doorway states. Theoretical calculations of $S(E)$ by use of the effective interactions NL2, NL3, DD-ME1, and DD-ME2 agree reasonably well, within a factor of ~ 3.5, in the limit $E \to 0$ (Fig. 2). Furthermore, the resonant behavior of the data cannot be described with the BP calculations because the effects of nuclear structure are neglected. However, an average description of the data (neglecting resonant oscillations) for the subbarrier region ($E \lesssim 6.0$ MeV) is reproduced satisfactorily. Such a description of an average S factor is quite sufficient because the reaction-rate formalism relies on the average S-factor behavior over the entire Gamow range.

In this context it is important to emphasize that the main purpose of this paper is not to investigate the oscillations in the ^{12}C+^{12}C fusion excitation function. To reproduce the resonances we could, for example, use the concept of internal and barrier waves based on a semiclassical description [39] or adopt the R matrix formalism (e.g., Michaud and Vogt [40]). However, neither theoretical approach would allow us to extrapolate with confidence the fusion cross section to the energy region of astrophysical interest.

To calculate the carbon burning rate, we use the values of $S(E)$ obtained on the basis of the well-established NL2 effective interaction. As one can see from Fig. 1, the ^{12}C density distribution obtained with the parameter set NL2 can describe satisfactorily the surface properties, which is the most important region for the fusion process at low energies. The values of $S(E)$ calculated at $E \leqslant 19.8$ MeV can be fitted by an analytic expression

$$S(E) = 5.15 \times 10^{16} \exp\left[-0.428\,E - \frac{3\,E^{0.308}}{1+e^{0.613(8-E)}}\right] \text{MeV b,} \quad (12)$$

where the center-of-mass energy E is expressed in mega-electron-volts. The formal maximum fit error, 16%, occurs at $E = 5.8$ MeV. However, let us bear in mind that the values of $S(E)$ provided by the NL2 model and given by Eq. (12) are actually uncertain within a factor of ~ 3.5.

With the aim of investigating the validity of our assumption for the real part of the nuclear interaction, we performed an optical-model (OM) analysis of the ^{12}C+^{12}C elastic-scattering data at energies around and slightly above the Coulomb barrier [41]. We defined the imaginary part of the optical potential, which accounts for the nuclear absorption process, as

$$W(r, E) = N_i V_N(r, E), \quad (13)$$

where $V_N(r, E)$ is described by Eq. (1), and we determined $N_i = 0.78$ by adjusting thirty elastic-scattering angular distributions corresponding to seven different heavy-ion systems and measured in a very wide energy range [42]. Figure 3 illustrates a comparison between our OM analysis and five elastic-scattering angular distribution data of the ^{12}C+^{12}C system. As one can note, it is possible to obtain a reasonable description of the data by adopting the São Paulo potential to account for the real part of the nuclear interaction, combined with a simple model to describe the imaginary part of the optical potential. This means that both elastic-scattering and fusion processes can be described by the same real part of the nuclear interaction, which has been well accounted for by the
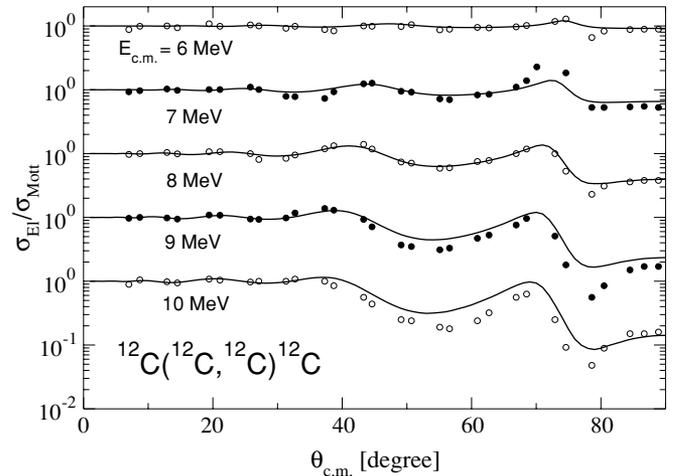
FIG. 3. Elastic-scattering angular distributions for the ^{12}C+^{12}C system at energies around and slightly above the Coulomb barrier [41]. The curves are the results of an OM calculation in which the São Paulo potential was assumed to describe the real part of the nuclear interaction, combined with a simple model to describe the imaginary part of the optical potential (see details in the text).

São Paulo potential, Eq. (1). As discussed in Ref. [42], details on the absorption part of the interaction are not very important for describing the elastic-scattering data, which allows us to get reasonable estimates for the ^{12}C+^{12}C system.

Further experiments at lower energies are necessary to confirm the validity of the predicted ^{12}C+^{12}C S factor and its impact on the reaction rate. However, the S factor is not the only uncertainty for a reliable description of the ^{12}C+^{12}C fusion process in stellar matter. The reaction rates are also uncertain because of the problems in calculating the probability of Coulomb BP in a dense many-body environment. We discuss these problems in Sec. III and show that the associated uncertainties are higher than the current uncertainties in the values of $S(E)$.

III. NUCLEAR FUSION RATE IN DENSE MATTER

A. Physical conditions and reaction regimes

In the following discussion we turn our attention to the plasma physics aspects of nuclear burning in dense matter. We will focus on the formalism of fusion reactions between identical nuclei $(A, Z) + (A, Z)$ in the wide domain of temperatures T and densities ρ, characteristic for the range of stellar environments outlined in the preceding section.

As an example, we consider the ^{12}C+^{12}C reaction in stellar matter at conditions displayed in the ρ–T phase diagram in Fig. 4. Under these conditions, carbon is fully ionized (either by electron pressure and/or by high temperature) and immersed in an almost uniform electron background. The electrons are typically strongly degenerate; their degeneracy temperature T_F is shown in the figure.

The state of ions (nuclei) is determined by the Coulomb coupling parameter $\Gamma = Z^2 e^2/(aT)$, where $a = [3/(4\pi n_i)]^{1/3}$ is the ion-sphere radius and n_i is the number density
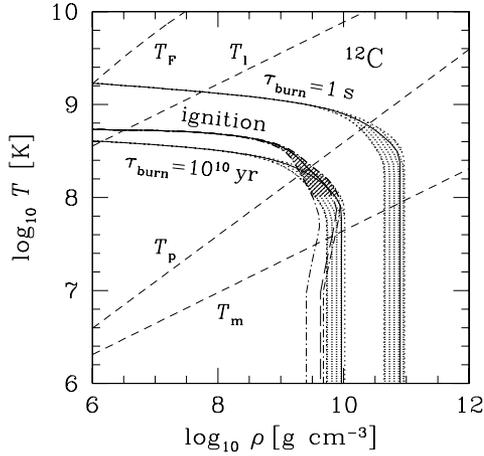
FIG. 4. Temperature-density diagram for carbon matter. Short-dashed curves show the electron degeneracy temperature T_F, the temperature T_l of the appearance of ion liquid, the melting temperature T_m of ion crystal, and the ion plasma temperature T_p. Solid curves correspond to the carbon burning times $\tau_{\text{burn}} = 1$ s and $\tau_{\text{burn}} = 10^{10}$ yr, and to carbon ignition; they are calculated with the most reliable model of carbon burning (Sec. III G). Hatched strips show theoretical uncertainties of these curves (limited by the minimum and maximum reaction-rate models). The long-dashed curve exhibits the unreliable part of the ignition curve; nearby thin dashed-and-dotted curves (to the right and left) indicate its assumed uncertainties.

of ions; the Boltzmann constant is set $k_B \equiv 1$. If $\Gamma \lesssim 1$ (which happens at $T \gtrsim T_l = Z^2 e^2/a$; see Fig. 4), the ions constitute a Boltzmann gas, whereas at higher Γ they constitute a strongly coupled Coulomb liquid. The gas transforms smoothly into the liquid, without any phase transition. At small T (large Γ) the liquid can solidify. In the density range displayed in Fig. 4, the solidification occurs at $T = T_m = Z^2 e^2/a\Gamma_m$, where $\Gamma_m = 175$ (e.g., De Witt *et al.* [43]). The important measure of quantum effects in ion motion is provided by the ion plasma frequency $\omega_p = \sqrt{4\pi Z^2 e^2 n_i/m}$ or the associated ion plasma temperature $T_p = \hbar\omega_p$ (m is the ion mass). As a rule, the quantum effects are strongly pronounced at T below T_p.

Figure 4 shows that the ion system can have very different properties, depending on T and ρ. As a result, there are five qualitatively different regimes of nuclear burning in dense matter (Salpeter and Van Horn [15]). These are (1) the classical thermonuclear regime, (2) the thermonuclear regime with strong plasma screening, (3) the thermopycnonuclear regime; (4) the thermally enhanced pycnonuclear regime, and (5) the zero-temperature pycnonuclear regime. The regimes differ mainly in the character of the Coulomb BP of reacting nuclei. The penetration can be greatly complicated by Coulomb fields of ions that surround the reacting nuclei. These fields are fluctuating and random (e.g., Alastuey and Jancovici [44]).

A strict solution of the BP problem should imply the calculation of the tunneling probability in a random potential, with subsequent averaging over an ensemble of random potentials. This program has not been fully realized so far. The exact theory should take into account a range of effects that can be subdivided (somewhat conventionally) into classical

and quantum ones. The classical effects are associated with classical motion of plasma ions and with the related structure of Coulomb plasma fields (including spatial and temporal variability of these fields). The quantum effects manifest themselves in ion motion (e.g., zero-point ion vibrations), quantum "widths" of ion trajectories during Coulomb BP, and quantum statistics of reacting nuclei. The effects of quantum statistics are usually small for the obvious reason that quantum tunneling lengths are typically much larger than nuclear radii. The smallness of these effects has been confirmed by Ogata [45] in path-integral Monte Carlo (PIMC) simulations.

The reaction rates in the classical thermonuclear regime are well known (e.g., Fowler, Caughlan, and Zimmerman [32]); they have been tested very successfully by the theory and observations of the evolution of normal stars. This theory is only shortly reviewed in the following subsection. The reaction rates in other regimes have been calculated by a number of authors in different approximations. In the following discussion we summarize the main results published after the seminal paper by Salpeter and Van Horn [15] (see that paper for references to earlier works). Let us stress that the reaction rate is a rapidly varying function of plasma parameters. In the most important density-temperature domain it varies over tens of orders of magnitude (Sec. IV). In this situation, a very precise calculation of the reaction rate is very difficult but not required for many applications.

B. Classical thermonuclear reaction rate

The classical thermonuclear regime takes place at sufficiently high T and low ρ so that the ions constitute a Boltzmann gas ($T \gg T_l$; Fig. 4). The tunnel probability (penetrability) through the Coulomb barrier depends on the energy of the interacting ions; the main contribution to the reaction rate comes from ion collisions with energies approximately equal to the Gamow peak energy E_{pk} (which is much higher than T). This regime is typical for all nuclear burning stages in "normal" stars (from the main sequence to presupernovas).

The thermonuclear reaction rate is expressed by

$$R_{\text{th}} = \frac{n_i^2}{2} 4 \sqrt{\frac{2E_{\text{pk}}}{3\mu}} \frac{S(E_{\text{pk}})}{T} \exp(-\tau), \qquad (14)$$

where $E_{\text{pk}} = T\tau/3$ is the Gamow peak energy and

$$\tau = \left(\frac{27\pi^2\mu Z_1^2 Z_2^2 e^4}{2T\hbar^2}\right)^{1/3} = \left(\frac{27\pi^2 m Z^4 e^4}{4T\hbar^2}\right)^{1/3} \qquad (15)$$

is the parameter that characterizes the penetrability $\sim\exp(-\tau)$. The parameter τ can be rewritten as

$$\tau = 3(\pi/2)^{2/3}(E_a/T)^{1/3}, \quad E_a \equiv m Z^4 e^4/\hbar^2. \qquad (16)$$

Now the reaction rate can be presented as

$$R_{\text{th}} = \frac{n_i^2}{2} S(E_{\text{pk}}) \frac{\hbar}{m Z^2 e^2} P_{\text{th}} F_{\text{th}}, \qquad (17)$$

where $\hbar/(mZ^2e^2)$ is a convenient dimensional factor, F_{th} is the exponential function, and P_{th} is the preexponent:

$$F_{th} = \exp(-\tau), \quad P_{th} = \frac{8\pi^{1/3}}{\sqrt{3}2^{1/3}}\left(\frac{E_a}{T}\right)^{2/3}. \quad (18)$$

The classical thermonuclear reaction rate decreases exponentially with decreasing T.

C. Thermonuclear burning with strong plasma screening

The thermonuclear regime with strong plasma screening operates in a colder and denser plasma ($T_p \lesssim T \lesssim T_l$), where ions constitute a strongly coupled classical Coulomb system (liquid or solid). The majority of ions in such a system are confined in deep Coulomb potential wells ($Z^2e^2/a \gtrsim T$). The main contribution into the reaction rate comes from a small amount of higher-energy, unbound ions with $E \approx E_{pk} \gg T$ from the tail of the Boltzmann distribution. The plasma screening effects are produced by surrounding plasma ions and simplify close approaches of the reacting nuclei, required for successful Coulomb tunneling. This enhances the reaction rate with respect to that given by Eqs. (17) and (18).

The enhancement has been studied by a number of authors, beginning with Salpeter [8]; it can reach many orders of magnitude. Calculations show that the equations given in Sec. III B remain valid in this regime, but the penetrability function F_{th} has to be corrected for the screening effects:

$$F_{th} = F_{sc}\exp(-\tau), \quad F_{sc} = \exp(h), \quad (19)$$

where F_{sc} is the enhancement factor and h is a function of plasma parameters.

Plasma screening effects are usually modeled by introduction of a mean-force plasma potential $H(r)$. In this approximation, the reacting nuclei move in a potential $W(r) = Z^2e^2/r - H(r)$. The mean-force plasma potential $H(r)$ is static and spherically symmetric. It cannot take into account dynamical variations of plasma microfields and their instantaneous spatial structures in the course of an individual tunneling event. In the mean-force approximation, the function h consists of two parts, $h = h_0 + h_1$, where the leading term $h_0 = H(0)/T$ ($\gg |h_1|$) is calculated assuming a constant plasma potential $H(r) = H(0)$ during the quantum tunneling, whereas h_1 is a correction that is due to a weak variation of $H(r)$ along the tunneling path. Note that according to simple estimates (e.g., Ref. [46]) typical tunneling lengths of reacting ions in the thermonuclear regime (where $T \gtrsim T_p$) are considerably smaller than the ion-sphere radius a, and typical tunneling times are much smaller than the plasma oscillation period $\sim\omega_p^{-1}$. This justifies the assumption of almost constant and static plasma potential during a tunneling event.

The mean-force plasma potential $H(r)$ for a classical strongly coupled system of ions (liquid or solid) can be determined by use of classical Monte Carlo (MC) sampling (e.g., DeWitt, Graboske, and Cooper [47]). MC sampling gives the static radial-pair distribution function of ions $g(r) = \exp[-W(r)/T]$ that enables one to find $H(r)$. In this way one can accurately determine $g(r)$ and $H(r)$ at not too small r (typically, at $r \gtrsim a$), because of poor MC statistics of close

ion separations. The potential $H(r)$ at small r, required for a tunneling problem, is obtained by extrapolation of MC values of $H(r)$ to $r \to 0$; the extrapolation procedure is a delicate subject and may be ambiguous (as discussed, e.g., by Rosenfeld [48]).

It is only $H(0)$ that is required for finding h_0. For a classical ion system, $H(0)$ can be determined by $H(0) = \Delta\mathcal{F}$, where $\Delta\mathcal{F}$ is a difference of Coulomb free energies (for a given system and for a system with two nuclei merging into one compound nucleus; e.g., DeWitt *et al.* [47]). In this approximation, the enhancement factor of the nuclear reaction becomes a thermodynamic quantity and acquires a Boltzmann form, $\exp(h_0) = \exp(\Delta\mathcal{F}/T)$, showing that plasma screening increases the probability of close separations (and subsequent quantum tunneling); h_0 becomes the function of one argument Γ. Assuming a linear mixing rule in a multicomponent strongly coupled ion system, Jancovici [49] obtained $h_0 = 2f_0(\Gamma) - f_0(2^{5/3}\Gamma)$, where $f_0(\Gamma)$ is a Coulomb free energy of one ion in a one-component plasma of ions (in units of T). In a Coulomb liquid at $\Gamma \gtrsim 1$ the linear mixing rule is highly accurate (DeWitt and Slattery [50]); the function $f_0(\Gamma)$ is now determined from MC sampling with very high accuracy (e.g., Refs. [50,51]). In this way the function $h_0(\Gamma)$ has been calculated in many papers (e.g., Refs. [46,48,49,52]), and the results are in very good agreement. Let us present the analytical approximation of $h_0(\Gamma)$ that follows from the recent MC results of DeWitt and Slattery [52] for a Coulomb liquid at $1 \leqslant \Gamma \leqslant 170$:

$$h_0 = 1.0563\Gamma + 1.0208\Gamma^{0.3231} - 0.2748\ln\Gamma - 1.0843. \quad (20)$$

However, this accurate expression is inconvenient for further use, and we propose another fit:

$$h_0 = C_{sc}\Gamma^{3/2}/[(C_{sc}/\sqrt{3})^4 + \Gamma^2]^{1/4}, \quad (21)$$

where $C_{sc} = 1.0754$. It approximates e^{h_0} with the maximum error of $\sim 40\%$ at $\Gamma = 170$, quite sufficient for our purpose. There may be still some uncertainty of the reaction rate associated with the choice of C_{sc}, but it seems to be no higher than the uncertainty in the S factor (Sec. II). Our fit function in Eq. (21) is chosen in such a way to reproduce also the well-known expression $h_0 \to \sqrt{3}\,\Gamma^{3/2}$ derived by Salpeter [8] for the classical thermonuclear regime ($\Gamma \ll 1$), where $h_0 \ll 1$ and the plasma screening is weak. In the Coulomb liquid, at $\Gamma \gtrsim 1$, we have actually the linear function $h_0 = C_{sc}\Gamma$. Such a function was obtained by Salpeter [8], who used a simple model of ion spheres (with a slightly lower coefficient, $C_{sc}^{Salp} = 1.057$).

Some authors calculated h_0 and the associated enhancement factor e^{h_0} by extrapolating MC $H(r)$ to $r \to 0$ (as just discussed). In particular, Ogata *et al.* [53,54] employed this formalism to study the enhancement of nuclear reactions in one-component and two-component strongly coupled ion liquids. The enhancement factor e^{h_0} for a one-component ion liquid, calculated in these papers {e.g., Eq. (6) in Ref. [53]}, is systematically higher than the factor given by Eq. (20) or (21). The difference reaches a factor of approximately 40 for $\Gamma \sim 170$. Because the enhancement factor itself becomes as high as $e^{h_0} \sim 10^{74}$ at $\Gamma \sim 170$, such a difference is insignificant for

many applications. As shown by Rosenfeld [48], the difference comes from the problems of extrapolation of $H(r)$ to $r \to 0$ in Refs. [53,54]. The function h_0 was also calculated by Ogata [45], who used the direct PIMC method. His result [his Eq. (19)] is in much better agreement with Eq. (20). The maximum difference of e^{h_0} reaches a factor of only approximately 6 at $\Gamma = 170$. Recently new PIMC calculations have been performed by Pollock and Militzer [55], but the authors have not calculated directly $h_0(\Gamma)$.

Let us emphasize that the enhancement factor e^{h_0}, derived in a constant mean-force plasma potential $H(0)$, is invariant with respect to the order of the mean-force averaging and the tunneling probability calculation. One can consider a real (random) plasma potential, constant over a tunneling path in an individual tunneling event. Calculating the tunneling probability and averaging over an ensemble of realizations of plasma potentials, one comes (e.g., Ref. [46]) to the same expression for h_0 as given by the mean-force potential.

In addition to e^{h_0}, the enhancement factor F_{sc} in Eq. (19) contains a smaller factor e^{h_1}, associated with variations of the plasma potential along the tunneling path. Numerous calculations of h_1 have commonly employed the mean-force potential $H(r)$. The results are sensitive to the behavior of $H(r)$ at small r (where this behavior is not very certain). For example, Jancovici [49] got $h_1 = -(5/32)\,\Gamma\,(3\Gamma/\tau)^2$. Note that, for the thermonuclear burning ($T \gtrsim T_p$, Sec. III A), the ratio $3\Gamma/\tau \approx r_t/a \sim (T/T_p)^{2/3}$ can be regarded as a small parameter (r_t being the tunneling length). It is possible that the mean-force approximation is too crude for calculating h_1. For that reason, we do not specify h_1 in this section. Our final expression for the reaction rate includes h_1, but phenomenologically, when we combine reaction rates in all regimes (Sec. III G).

D. Zero-temperature pycnonuclear fusion

The zero-temperature pycnonuclear regime operates in a cold and dense matter (T well below T_p) in a strongly coupled quantum system of nuclei. In this regime the Coulomb barrier is penetrated owing to zero-point vibrations of neighboring nuclei that occupy their ground states in a strongly coupled system. One usually considers pycnonuclear reactions in a crystalline lattice of nuclei but they are also possible in a quantum liquid. The main contribution to the reaction rate comes from pairs of nuclei that are most closely spaced. The reaction rate is temperature independent but increases exponentially with increasing density, as we discuss in the following text.

Pycnonuclear reaction rates between identical nuclei in crystalline lattice have been calculated by many authors using different approximations. In analogy with Eq. (17), the resulting reaction rates can be written as

$$R_{pyc} = \frac{n_i^2}{2} S(E_{pk}) \frac{\hbar}{m Z^2 e^2} P_{pyc} F_{pyc}, \qquad (22)$$

where F_{pyc} and P_{pyc} depend on the density and have the form

$$F_{pyc} = \exp(-C_{exp}/\sqrt{\lambda}), \quad P_{pyc} = 8\,C_{pyc}\,11.515/\lambda^{C_{pl}}. \quad (23)$$

The dimensionless parameters C_{exp}, C_{pl}, and C_{pyc} are model dependent (see subsequent discussion). The dimensionless parameter λ is expressed in terms of the mass fraction X_i contained in atomic nuclei (in a one-component ion plasma under study) and the mass density ρ of the medium:

$$\lambda = \frac{\hbar^2}{m Z^2 e^2} \left(\frac{n_i}{2}\right)^{1/3} = \frac{1}{A Z^2} \left(\frac{1}{A} \frac{\rho X_i}{1.3574 \times 10^{11}\,\mathrm{g\,cm^{-3}}}\right)^{1/3}. \qquad (24)$$

For densities ρ lower than the neutron drip density ($\sim 4 \times 10^{11}$ g cm^{-3}; e.g., Ref. [56]), one can set $X_i = 1$, whereas for higher ρ one has $X_i < 1$ because of the presence of free (dripped) neutrons.

The reaction rate can be expressed numerically as

$$R_{pyc} = \rho X_i A Z^4 S(E_{pk}) C_{pyc} 10^{46} \lambda^{3-C_{pl}}$$
$$\times \exp(-C_{exp}/\sqrt{\lambda})\mathrm{s}^{-1}\,\mathrm{cm}^{-3}, \qquad (25)$$

where ρ is in grams percubic centimeter and $S(E_{pk})$ is in mega-electron-volts times barns. The typical energy of the interacting nuclei is $E_{pk} \sim \hbar\omega_p$.

Table I lists the values of C_{exp}, C_{pl}, and C_{pyc} reported in the literature for two models (1 and 2) of Coulomb BP by Salpeter and Van Horn [15], for six models (3–8) by Schramm and Koonin [16], and for one model (9) by Ogata, Iyetomi, and Ichimaru [53]. The corresponding carbon burning rates are plotted as functions of density in Fig. 5. In this figure (as well as in Figs. 4 and 6) we use the astrophysical factors given by fit expression (12). Actually, the S factors are uncertain within one order of magnitude (Sec. II) but we ignore these uncertainties (because they seem to be much lower than those associated with the Coulomb BP).

All the authors just cited have treated quantum tunneling by fixing the center of mass of reacting nuclei in its equilibrium position. All models, except for models 5–8, focus on nuclear reactions in the body-centered-cubic (bcc) lattice of atomic nuclei. This lattice is thought to be preferable over other lattices, particularly, over the face-centered-cubic (fcc) lattice. The main reason is that the bcc lattice is more tightly bound in the approximation of a rigid electron background. However, the difference in binding energies of bcc and fcc lattices is small (see, e.g., Ref. [16]), and a finite polarizability of the electron background complicates the problem [57]. Therefore one cannot exclude that the lattice type is fcc.

Salpeter and Van Horn [15] calculated the quantum tunneling probability of interacting nuclei in a bcc Coulomb lattice by using the three-dimensional WKB approximation (most adequate for the given problem). The authors employed two models, *static* and *relaxed* lattice (models 1 and 2 in Table I), to account for the lattice response to the motion of tunneling nuclei. The static-lattice model assumes that surrounding nuclei remain in their original lattice sites during the tunneling process. The relaxed-lattice model assumes that the surrounding nuclei are promptly rearranged into new equilibrium positions in response to the motion of the reacting nuclei. Simple estimates show that the actual tunneling is dynamical (neither static not relaxed). Thus the static-lattice and relaxed-lattice models impose constraints on the actual reaction rate. In Ref. [15] the screening potential

TABLE I. Coefficients C_{exp}, C_{pyc}, and C_{pl} of the pycnonuclear reaction rate obtained at $T = 0$ [see Eq. (25)]. The dimensionless parameter C_T, which is related to the "renormalized" temperature [Eq. (29)], is also included.

Model no.	C_{exp}	C_{pyc}	C_{pl}	C_T	Model	Refs.
1	2.638	3.90	1.25	0.724	bcc; static lattice	[15,16]
2	2.516	4.76	1.25	0.834	bcc; relaxed lattice—Wigner-Seitz	[15,16]
3	2.517	4.58[a]	1.25	0.834	bcc; relaxed lattice	[16]
4	2.659	5.13[a]	1.25	0.707	bcc; effective mass approx.	[16]
5	2.401	7.43[a]	1.25	0.960	fcc; static lattice	[16]
6	2.265	13.5[a]	1.25	1.144	fcc; relaxed lattice—Wigner-Seitz	[16]
7	2.260	12.6[a]	1.25	1.151	fcc; relaxed lattice	[16]
8	2.407	13.7[a]	1.25	0.953	fcc; effective mass approx.	[16]
9	2.460	0.00181	1.809	0.893	bcc; MC calculations	[53]
10	2.450	50	1.25	0.904	Maximum rate	Present paper
11	2.650	0.5	1.25	0.711	Minimum rate	Present paper

[a]Corrected for the curvature factor as explained in the text.

for the relaxed-lattice model was calculated approximately; the energy difference between the initial state and the fused state was evaluated by subtraction of the energies of the corresponding Wigner-Seitz (WS) spheres. The relaxed lattice simplifies Coulomb tunneling and increases the reaction rate with respect to the static lattice (cf., curves 1 and 2 in Fig. 5).

Schramm and Koonin [16] applied this treatment to the bcc and fcc, static and relaxed lattices in the same WKB approximation. They calculated the screening potential for the relaxed lattice model with improved accuracy (model 3 of Table I for the bcc lattice and model 7 for fcc). For comparison, they also used the screening potential for the relaxed lattice obtained in the WS approximation (as in Ref. [15]). Unfortunately, when they calculated the tunneling probability they neglected the correction e^K for the "curvature

of trajectories" of reacting ions. This is the main reason for the formal disagreement between the results of Salpeter and Van Horn [15] and Schramm and Koonin [16] for the static-lattice and relaxed-lattice WS models (1 and 2) of bcc crystals. The inclusion of the curvature correction should reduce the constant C_{pyc} in Eq. (25) and the reaction rates calculated in Ref. [16]. Fortunately, one can extract this correction by comparing Eq. (38) of Ref. [15] with Eq. (31) of Ref. [16]. In this way we get $e^K = 0.067$ for the static bcc lattice, and

FIG. 6. Temperature dependence of the carbon fusion rate at $\rho = 5 \times 10^9$ g cm^{-3}. Solid curve 1 is our most optional interpolation expression (Sec. III G), based on model 1 from Table I with $\Lambda = 0.5$. Double hatched region shows theoretical uncertainties of model 1 associated with variations of Λ from 0.35 to 0.65. The dashed-and-dotted curve K is the interpolation of Kitamura [62]. Short-dashed curve 1 is calculated from the expressions of Salpeter and Van Horn [15], which are valid in the pycnonuclear regime ($T = 0$ and with the thermal enhancement). Long-dashed curves show the thermonuclear reaction rates calculated with plasma screening, (Sec. III C) and without screening (Sec. III B) taken into account. Single hatched region displays total assumed theoretical uncertainties of the reaction rates.

FIG. 5. Rates of pycnonuclear carbon burning at $T = 0$ as functions of density for the different theoretical models (from Table I). Solid and dashed curves refer to the burning in bcc and fcc crystals, respectively; the dashed-and-dotted curve K is the model by Kitamura [62] (for bcc crystals). Hatched strip shows assumed uncertainties of the reaction rates for bcc crystals (limited by models 10 and 11 from Table I).

$e^K = 0.050$ for the relaxed WS bcc lattice. After this correction is introduced into the coefficients C_{pyc}, obtained formally from the results of Schramm and Koonin, these coefficients become identical to those given by Salpeter and Van Horn. Thus Schramm and Koonin actually exactly reproduce models 1 and 2 of Salpeter and Van Horn. The curvature correction for models 3–8 of Schramm and Koonin have not been determined. We expect it to be $e^K \approx 0.050$ for model 3 and $e^K = 0.067$ for model 4 (bcc crystals), and we introduced such corrections in Table I. We introduced, somewhat arbitrarily, the correction $e^K = 0.05$ in all fcc lattice models 5–8.

The two versions of the screening potential for the relaxed lattice (WS and more accurate) almost coincide. Accordingly, models 2 and 3 yield almost the same reaction rates for the bcc lattice, and models 6 and 7 yield nearly identical rates for the fcc lattice (Fig. 5).

Schramm and Koonin [16] also took into account the dynamical effect of motion of the surrounding ions in response to the motion of tunneling nuclei in the relaxed lattice (models 4 and 8). This effect was described by introduction of the effective mass of the reacting nuclei. The effective mass appears to be noticeably higher than the real nucleus mass, reducing the tunneling probability. It turns out that the reduction almost exactly compensates for the increase of the tunneling probability that is due to the lattice relaxation, neglecting the effective-mass effects [15]. Accordingly, model 4 of Schramm and Koonin [16] gives almost the same reaction rate as model 1 (for bcc); and model 8 gives almost the same rate as model 5 (for fcc). This means that the two limiting approximations, the static lattice and relaxed lattice, yield very similar reaction rates. It is natural to expect that the actual reaction rate (to be calculated for the dynamically responding lattice) would be the same, and the problem of dynamical tunneling is thus solved [16]. Note that this conclusion is made with the curvature corrections e^K already adopted (whereas the accurate curvature correction for the effective-mass model has not been calculated).

Zero-temperature pycnonuclear reactions in bcc crystals were also studied by Ogata *et al.* [53] and Ichimaru, Ogata, and Van Horn [58], who used MC lattice screening potentials. These authors considered one-component and two-component ion systems. Model 9 of Table I represents their results for one-component bcc crystals. To calculate the tunneling probability, the authors used the mean-force plasma screening potential $H(r)$, obtained from MC sampling in a classical bcc crystal at $r \gtrsim a$ and extrapolated to $r \to 0$ (see Sec. III C). This potential is static and spherically symmetric. It cannot take into account the dynamics of lattice response and the anisotropic character of the real screening potential in a lattice. Furthermore, the BP was calculated by numerical solution of the effective radial Schrödinger equation. This procedure is more approximate than the direct WKB approach of Salpeter and Van Horn [15] and Schramm and Koonin [16] (In particular, it neglects the curvature corrections). Numerically, Ogata *et al.* [53] give a reaction rate that is close to that of the relaxed-lattice model (model 2) of Salpeter and Van Horn [15]. The main reason for the coincidence of these rates is that the screening potential in the radial equation of

Ogata *et al.* is close to the relaxed-lattice screening potential of Salpeter and Van Horn at ion separations $r \sim 1.5\,a$, which is most important for pycnonuclear tunneling problem (see Fig. 2 in Ref. [53]).

In spite of the differences in theoretical models 1–9, they result in similar reaction rates (Fig. 5). According to the preceding discussion, models 1 and 4 seem to be the most reliable among all available models for the bcc lattice, whereas models 5 and 8 seem to be the most reliable for fcc. These reaction rates may be modified, for instance, by taking into account the quantum effect of the spreading of WKB trajectories or by a more careful treatment of the center-of-mass motion of reacting nuclei. Such effects will possibly reduce the reaction rate (as discussed in Ref. [55] with regard to the spreading of WKB trajectories). This could have been studied by direct PIMC simulations (e.g., Refs. [45,55]). PIMC is also a good tool to confirm the conclusions on dynamical effects of lattice response. However, PIMC is time consuming and requires very powerful computers. It is not clear whether today's computer capabilities are sufficient for obtaining accurate PIMC pycnonuclear reaction rates.

We suggest calculating the reaction rates from Eq. (25), taking into account that the constants C_{exp}, C_{pl}, and C_{pyc} are not known very precisely. In particular, we propose two "limiting" purely phenomenological sets of these constants, labeled as models 10 and 11 in Table I. These limiting parameters define the maximum and minimum reaction rates that enclose all model reaction rates 1–4 and 9 (proposed in the literature for the bcc lattice in a density range where the pycnonuclear carbon burning is important). They also enclose the most reliable models, 5 and 8, for the fcc lattice.

The crucial parameter for modeling pycnonuclear fusion is the exponent $F_{pyc} = \exp(-C_{pyc}/\sqrt{\lambda})$ in Eqs. (23) that characterizes the probability of Coulomb tunneling. It is easy to show that the exponent argument behaves as $C_{pyc}/\sqrt{\lambda} = \alpha (r_{12}/r_{qm})^2 \propto \rho^{-1/6}$, where r_{12} is the equilibrium distance between the interacting nuclei in their lattice sites, r_{qm} is the rms displacement of the nucleus that is due to zero-point vibrations in its lattice site, and $\alpha \sim 1$ is a numerical factor that depends on a model of Coulomb tunneling. The usual condition is $r_{qm} \ll r_{12}$ (and the tunneling length $\gg r_{qm}$). The exponent argument $C_{pyc}/\sqrt{\lambda}$ is typically large but decreases with growing ρ, making the Coulomb barrier more transparent. The tunneling is actually possible for closest neighbors (smallest r_{12}); the tunneling of more distant nuclei (higher r_{12}) is exponentially suppressed. Elastic lattice properties specify r_{qm} and α and are thus most important for the reaction rate. The presence of different ion species, lattice impurities, and imperfections may drastically affect the rate [15].

E. Thermally enhanced pycnonuclear regime

Thermally enhanced pycnonuclear burning occurs with increasing T; it operates [15] in a relatively narrow temperature interval, $0.5 T_p / \ln(1/\sqrt{\lambda}) \lesssim T \lesssim 0.5 T_p$. In this interval the majority of the nuclei occupy their ground states in a strongly

coupled quantum Coulomb system, but the main contribution to the reaction rate comes from a tiny fraction of nuclei that occupy excited bound energy states. The increase of the excitation energy increases the penetrability of the Coulomb barrier and makes the excited states more efficient than the ground state.

The thermally enhanced pycnonuclear regime has been studied less accurately than the zero-temperature pycnonuclear regime. Salpeter and Van Horn [15] calculated the thermally enhanced pycnonuclear reaction rate for models 1 and 2 of a bcc lattice in the WKB approximation. The spectrum of excited quantum states was determined for a relative motion of interacting nuclei in an anisotropic harmonic-oscillator field; the summation over discrete quantum states in the expression for the reaction rate was replaced with the integration. According to their Eq. (45), the enhancement of the reaction rate is approximately described by

$$\frac{R_{\mathrm{pyc}}(T)}{R_{\mathrm{pyc}}(0)} - 1 = \frac{\Omega}{\lambda^{1/2}} \exp\left(-\Lambda \frac{T_p}{T} + \frac{\Omega_1}{\sqrt{\lambda}} e^{-\Lambda_1 T_p/T}\right), \quad (26)$$

where Ω, Ω_1, Λ, and Λ_1 are model-dependent dimensionless constants. The exponent $\exp(-\Lambda T_p/T)$ reflects the Boltzmann probability of occupying excited quantum states, and the double exponent $\exp[(\Omega_1/\sqrt{\lambda})e^{-\Lambda_1 T_p/T}]$ describes the enhancement itself. In this case the characteristic energy of the reacting nuclei is

$$E_{\mathrm{pk}} \approx C_1 \hbar \omega_p + C_2 \frac{Z^2 e^2}{a} \exp\left(-\Lambda_1 \frac{T_p}{T}\right), \quad (27)$$

where C_1 and C_2 are new dimensionless constants (~ 1). When T increases from $T = 0$ to $T \sim 0.5 T_p$, the characteristic energy E_{pk} increases from the ground-state level, $E_{\mathrm{pk}} \sim \hbar \omega_p$, to the top of the Coulomb potential well, $E_{\mathrm{pk}} \sim Z^2 e^2/a$.

The thermally enhanced pycnonuclear reaction rate was studied also by Kitamura and Ichimaru [59], who adopted the formalism of Ogata, *et al.* [53] (Secs. III C and III D). The relative motion of interacting nuclei was described by a model radial Schrödinger equation that employed the angle-averaged static MC plasma screening potential. The excited energy states were determined from the solution of this equation. Such an approach seems to be oversimplified. It gives the temperature dependence of the reaction rate {Eqs. (14) and (15) in Ref. [58]} that, functionally, differs from the temperature dependence, Eq. (27), predicted by Salpeter and Van Horn. Nevertheless, numerically both temperature dependencies at $T \lesssim 0.5 T_p$ are in a reasonable qualitative agreement.

We expect that the reaction rate in the thermally enhanced pycnonuclear regime will be further elaborated in the future.

F. The intermediate thermopycnonuclear regime

The intermediate thermopycnonuclear regime is realized at temperatures $T \sim T_p$ (roughly, at $T_p/2 \lesssim T \lesssim T_p$) that separate the domains of quantum and classical ion systems. The main contribution to the reaction rate stems then from nuclei that are either slightly bound or slightly unbound with respect to their potential wells. The calculation of the reaction

rate in this regime is complicated. We describe this rate by a phenomenological expression presented in the following subsection.

G. Single analytical approximation in all regimes

Let us propose a phenomenological expression for the reaction rate that combines all the five burning regimes:

$$R = R_{\mathrm{pyc}}(T = 0) + \Delta R(T),$$

$$\Delta R(T) = \frac{n_i^2}{2} S(E_{\mathrm{pk}}) \frac{\hbar}{m Z^2 e^2} P F,$$

$$F = \exp\left(-\widetilde{\tau} + C_{\mathrm{sc}} \widetilde{\Gamma} \, \varphi \, e^{-\Lambda T_p/T} - \Lambda \frac{T_p}{T}\right),$$

$$P = \frac{8 \pi^{1/3}}{\sqrt{3} \, 2^{1/3}} \left(\frac{E_a}{\widetilde{T}}\right)^{\gamma}. \quad (28)$$

In this case, $\varphi = \sqrt{\Gamma}/[(C_{\mathrm{sc}}^4/9) + \Gamma^2]^{1/4}$; $R_{\mathrm{pyc}}(T = 0)$ is the zero-temperature pycnonuclear reaction rate (Sec. III D); $\Delta R(T)$ is the temperature-dependent part (with a product of an exponential function F and a preexponent P). The quantities $\widetilde{\tau}$ and $\widetilde{\Gamma}$ are similar to the familiar quantities τ and Γ, but contain a "renormalized" temperature $\widetilde{T}$:

$$\widetilde{\tau} = 3 \left(\frac{\pi}{2}\right)^{2/3} \left(\frac{E_a}{\widetilde{T}}\right)^{1/3}, \quad \widetilde{\Gamma} = \frac{Z^2 e^2}{a \widetilde{T}}, \quad \widetilde{T} = \sqrt{T^2 + C_T^2 T_p^2}, \quad (29)$$

where C_T is a dimensionless renormalization parameter (~ 1). For high temperatures, $T \gg T_p$, we have $\widetilde{\tau} \to \tau$, $\widetilde{\Gamma} \to \Gamma$, and $\widetilde{T} \to T$. In this case the temperature-dependent term tends to $\Delta R(T) \to R_{\mathrm{th}}(T) \gg R_{\mathrm{pyc}}$, and Eqs. (29) reproduce the thermonuclear reaction rate (Secs. III B and III C). At low temperatures, $T \lesssim T_p$, the quantities $\widetilde{\tau}$, $\widetilde{\Gamma}$, and $\widetilde{T}$, roughly speaking, contain "the quantum temperature" T_p rather than the real temperature T in the original quantities τ, Γ, and T. In the limit of $T \to 0$ we obtain $\widetilde{\Gamma} = 1/[\sqrt{\lambda} (72\pi)^{1/6} C_T]$ and $\widetilde{\tau} = (3\sqrt{\pi/\lambda})/(2^{7/6} C_T^{1/3})$.

At this point, let us require that, at $T \ll T_p$ the factor $\exp(-\widetilde{\tau})$ in the exponential function F, Eqs. (29), reduce to $\exp(-C_{\mathrm{exp}}/\sqrt{\lambda})$ in the exponential function F_{pyc}, Eqs. (23). This would allow us to obey Eq. (26) by satisfying the equality

$$3\sqrt{\pi}/(2^{7/6} C_T^{1/3}) = C_{\mathrm{exp}}. \quad (30)$$

Taking C_{exp}, we can determine C_T (see Table I). The double exponent factor in F, Eqs. (28), will correspond to the double exponent factor in Eq. (26). Strictly speaking, Eq. (26) contains two different constants, Λ and Λ_1. However, taking into account the uncertainties of R in the thermally enhanced pycnonuclear regime (Sec. III E), we replace two constants with one.

Finally, the quantity γ in Eqs. (29) should be taken in such a way as to reproduce the correct limit $\gamma_1 = 2/3$ at $T \gg T_p$ (Sec. III B) and $\gamma_2 = (2/3)(C_{\mathrm{pl}} + 0.5)$ at $T \ll T_p$ [see Eq. (26)]. The natural interpolation expression for γ would be

$$\gamma = \left(T^2 \gamma_1 + T_p^2 \gamma_2\right)/\left(T^2 + T_p^2\right). \quad (31)$$

In addition, we need the reaction energy E_{pk} to evaluate the astrophysical factor $S(E_{pk})$. Because the S factor is a slowly varying function of energy, it is reasonable to approximate E_{pk} by the expression

$$E_{pk} = \hbar\omega_p + \left(\frac{Z^2 e^2}{a} + \frac{T\tau}{3}\right) \exp\left(-\frac{\Lambda T_p}{T}\right), \quad (32)$$

which combines the expressions in the thermonuclear and pycnonuclear regimes. To avoid the introduction of many fit parameters (unnecessary at the present state of investigation), we set $C_1 = C_2 = 1$ in expression (27).

Thus we propose to adopt analytic expressions (29) by using the following parameters:

(1) $C_{sc} = 1.0754$ for the case of strong plasma screening in the thermonuclear regime (Sec. III C);
(2) C_{exp}, C_{pyc}, and C_{pl} for conditions of zero-temperature pycnonuclear burning (see Table I and Sec. III D);
(3) The quantum-temperature constant C_T (Sec. III D), which is important at $T \sim T_p$ and expressed through C_{exp} by means of Eq. (30); the corresponding values of C_T are listed in Table I;
(4) The last constant Λ, which is important at $T \sim T_p$, is still free.

We have checked (Fig. 6) that taking the optional model 1 from Table I and the value $\Lambda = 0.5$ results in a good agreement with the carbon burning rate calculated at $\rho \sim 10^9$–10^{10} g cm^{-3} and $T \lesssim 0.5T_p$ from Eq. (45) of Salpeter and Van Horn [15] (for the thermally enhanced pycnonuclear regime). (Note that model 2 requires slightly lower $\Lambda \approx 0.45$.) Taking $\Lambda = 0.35$ leads to a noticeably higher reaction rate at $T \lesssim 0.5T_p$, while taking $\Lambda = 0.65$ leads to a noticeably lower rate.

Accordingly, for any model of zero-temperature pycnonuclear burning from Table I we suggest adopting $\Lambda = 0.5$ as optional, with $\Lambda = 0.35$ to maximize and $\Lambda = 0.65$ to minimize the reaction rate. In particular, model 1 with $\Lambda = 0.5$ seems to be the "most optional"; our limiting model 10 from Table I with $\Lambda = 0.35$ is expected to give the upper theoretical limit for the reaction rate, whereas the other limiting model 11 with $\Lambda = 0.65$ is expected to give the lower theoretical limit. We also need the astrophysical factor $S(E)$, which was described in Sec. II, for the carbon burning. We could easily introduce additional constants to tune our phenomenological model when precise calculations of reaction rates appear in the future.

For illustration, Fig. 6 shows the temperature dependence of the carbon burning rate at $\rho = 5 \times 10^9$ g cm^{-3}. The solid curve is the most optimal model (based on both—zero-temperature and thermally enhanced—pycnonuclear burning models of Salpeter and Van Horn [15] for the bcc static lattice). The double-hatched region shows assumed uncertainties of this model associated with variations of Λ from 0.35 to 0.65 (as if we accept the zero-temperature model but question the less elaborated model of thermal enhancement). The single hatched region indicates overall uncertainties (limited by the models of the maximum and minimum reaction rates). We obtain the lower long-dashed curve assuming classical

thermonuclear burning without any screening (Sec. III B). We calculate the upper long-dashed curve by using the formalism of thermonuclear burning with screening (Sec. III C). The screening enhancement of the reaction rate becomes stronger with the decrease of T. The formalism for describing this enhancement is expected to be valid at $T \gtrsim T_p$, but we intentionally extend the upper long-dashed curve to $T = 0.5 T_p$, where the formalism breaks down and the curve diverges from the expected (solid) curve. The short-dashed curve is calculated from the equations of Salpeter and Van Horn [15] derived in the thermally enhanced pycnonuclear regime (model 1) and valid at $T \lesssim 0.5T_p$. We intentionally extend the curve to higher T, where the formalism of thermally enhanced pycnonuclear burning becomes invalid and the curve diverges from the expected curve. Our phenomenological solid curve provides a natural interpolation at $T \sim T_p$ between the short-dashed curve and the upper long-dashed curve.

More complicated expressions for the reaction rate R in wide ranges of ρ and T were proposed by Kitamura [57], who combined the results of recent calculations of R in the different regimes. His expressions are mainly based on the results of Refs. [45,53,54,57,59], which are not free of approximations (as discussed in Secs. III C, III D, and III E). In contrast to our formula, Kitamura's formula took into account the effects of electron screening (finite polarizability of the electron gas), and he considered the case of equal and nonequal reacting nuclei. However, the electron screening effects are relatively weak; their strict inclusion in the pycnonuclear regime represents a complicated problem. We do not include them but, instead, take into account theoretical uncertainties of the reaction rates without electron screening. We have checked that the results by Kitamura [57] for carbon burning in the most important $T - \rho$ domain lie well within these uncertainties.

Our formula gives a smooth behavior of the reaction rate as a function of temperature and density, without any jump at the melting temperature $T = T_m$. We do not expect a strong jump of any such kind because the liquid-solid phase transition in dense stellar matter is tiny. A careful analysis shows the absence of noticeable jumps of transport coefficients [60] and the neutrino emissivity owing to electron-nucleus bremsstrahlung. A direct example is given by the theory of nuclear burning. Ichimaru and Kitamura [61] predicted a noticeable jump of the reaction rate at $T = T_m$, whereas a more careful analysis by Kitamura [57] considerably reduced this jump.

IV. CARBON BURNING AND IGNITION IN DENSE MATTER

In this section we analyze the rate of the ^{12}C+^{12}C reaction as a function of T and ρ and investigate the conditions for carbon burning in dense stellar matter.

Because the probability for Coulomb tunneling depends exponentially on plasma parameters, changes in density ρ and temperature T have dramatic effects on the burning rate R. In thermonuclear regimes (Secs. III B and III C) the ^{12}C+^{12}C rate is more sensitive to changes in temperature T than in density ρ. On the contrary, in pycnonuclear regimes (Secs. III D

and III E) the rate depends significantly on the density ρ. For instance, if T decreases from 3×10^9 K to 3×10^8 K at $\rho = 5 \times 10^9$ g cm^{-3} (Fig. 6; thermonuclear burning with strong screening), the reaction rate drops by ~ 20 orders of magnitude. when the enhancement that is due to plasma screening, is neglected, the rate will drop by 10 more orders of magnitude. An increase in density ρ from 10^8 to 10^{11} g cm^{-3} at $T \lesssim 3 \times 10^7$ K (in the zero-temperature pycnonuclear regime) results in a rate increase of ~ 100 orders of magnitude (Fig. 5). Note that no carbon can survive in a degenerate matter at $\rho > 3.90 \times 10^{10}$ g cm^{-3} because of the double electron capture $^{12}_6\text{C} \rightarrow ^{12}_5\text{B} \rightarrow ^{12}_4\text{Be}$ (e.g., Shapiro and Teukolsky [55]). The electron capture has a well-defined density threshold, 3.9×10^{10} g cm^{-3}, and proceeds quickly after the threshold is exceeded. We ignore this process in this section.

The strong dependence of the rate R on density ρ and temperature T leads to huge variations of the characteristic time scale $\tau_{\text{burn}} = n_i/R$ for carbon burning. Figure 4 shows two solid curves in the $\rho - T$ plane, along which $\tau_{\text{burn}} = 1$ s and 10^{10} years (nearly the universe age), respectively. They are calculated with the most optional carbon burning model (model 1 from Table I, $\Lambda = 0.5$). The curves are almost horizontal in the thermonuclear burning regime (R is a slowly varying function of ρ) and almost vertical in the pycnonuclear regime (R is a slowly varying function of T). The bending part of the curves corresponds to the thermally enhanced pycnonuclear and intermediate thermopycno nuclear regimes. At T and ρ above the upper line the burning time is even shorter than 1 s; at these conditions no carbon will survive in the dense matter of astrophysical objects. For conditions below the lower solid curve, τ_{burn} is longer than 10^{10} years, and carbon burning can be disregarded for most applications.

Thus the studies of carbon burning can be focused on the narrow strip in the $\rho - T$ plane between the lines of $\tau_{\text{burn}} = 1$ s and $\tau_{\text{burn}} = 10^{10}$ yr. Hatched regions show theoretical uncertainties of each curve (limited by the maximum and minimum reaction-rate models; Sec. III G). The uncertainties are relatively small in the thermonuclear regime where all models give nearly the same reaction rate. The uncertainties are higher in other burning regimes.

Having a carbon burning model, we can plot the carbon ignition curve. This curve is a necessary ingredient for modeling nuclear explosions of massive white dwarfs (producing supernova Ia events, so important for cosmology; see, e.g., Refs. [6,63]) and for modeling carbon explosions of matter in accreting neutron stars (feasible models of superbursts observed recently from some accreting neutron stars; e.g., Refs. [10–12]).

The ignition curve is commonly determined as the line in the $\rho - T$ plane (Fig. 4), where the nuclear energy generation rate is equal to the local neutrino emissivity of dense matter (the neutrino emission carries the generated energy out of the star). At higher ρ and T (above the curve) the nuclear energy generation rate exceeds the neutrino losses and carbon ignites. In Fig. 4 we present the carbon ignition (solid) curve, which we calculated by using the most optional model of carbon burning, together with its uncertainties (limited by the minimum and maximum rate models). The neutrino energy

losses are assumed to be produced by plasmon decay and by electron-nucleus bremsstrahlung. The neutrino emissivity that is due to plasmon decay is obtained from extended tables calculated by M. E. Gusakov (unpublished); they are in good agreement with the results by Itoh *et al.* [64]. The neutrino bremsstrahlung emissivity is calculated with the formalism of Kaminker *et al.* [65], which takes into account electron band-structure effects in crystalline matter.

For $\rho \lesssim 10^9$ g cm^{-3} theoretical uncertainties of the ignition curve are seen to be small. They become important at $\rho \gtrsim 10^9$ g cm^{-3} and $T \sim (1 - 3) \times 10^8$ K in the intermediate thermopycnonuclear burning regime and the thermally enhanced burning regime. This $\rho - T$ range is appropriate for central regions of massive and warm white dwarfs that may produce type Ia supernova explosions. Lower T are also interesting for these studies (e.g., Baraffe, Heger, and Woosley [7]).

If we formally continue the ignition curve to lower T, it will bend and shift to lower densities, where the nuclear burning time scale τ_{burn} is exceptionally slow, exceeding the age of the universe. The bend is associated with a very weak neutrino emission at $T \lesssim 10^8$ K. These parts of the ignition curve are oversimplified because at low T the energy outflow produced by thermal conduction becomes more efficient than the outflow that is due to neutrino emission. These parts are shown by the long-dashed curve (and their uncertainties are indicated by thin dashed-and-dotted curves). Unfortunately, the conduction energy outflow is nonlocal and "nonuniversal". It depends on specific conditions of the burning environment (a white dwarf core or a neutron star crust) and the associated thermal conductivity (provided mainly by strongly degenerate electrons). In this case the ignition becomes especially complicated. A very crude estimate shows that the ignition curve, governed by the thermal conduction, is nearly vertical and close to the $\tau_{\text{burn}} = 10^{10}$ yr curve in the range of T from 10^8 to 10^6 K in Fig. 4. At $T \lesssim 10^6$ K the curve is strongly affected by the thermal conductivity model. In a cold ideal carbon crystal, umklapp processes of electron-phonon scattering are frozen out (e.g., Ref. [66]). Under these conditions the electron conduction is determined by inefficient normal electron-phonon scattering, leading to high conductivity values. This shifts the ignition to higher ρ. On the other hand, carbon matter may contain randomly located ions of other elements (charged impurities) that can keep the electron Coulomb scattering rather efficient and maintain a low electron thermal conductivity. In this case the ignition curve at $T \lesssim 10^6$ K remains nearly vertical.

V. CONCLUSION

Our goal in this paper was to develop a phenomenological formalism for calculating fusion reaction rates between identical nuclei. This formalism should be applicable for a broad range of thermonuclear and pycnonuclear burning cases. It involves a generalized treatment for calculation of the fusion probability at low energies and the development of a single simple phenomenological expression for the fusion rate valid in a wide range of temperatures and densities.

We have introduced a generalized model approach for calculating the *S* factor of heavy-ion fusion reactions relevant for stellar nucleosynthesis processes. We have demonstrated the applicability and reliability of the approach by calculating the astrophysical factor $S(E)$ for the carbon fusion reaction $^{12}C+^{12}C$ (Sec. II) and by comparing the theoretical results with experimental data.

Furthermore, we have analyzed (Sec. III) previous calculations of the fusion rate for identical nuclei in stellar matter, with emphasis on the complicated problem of Coulomb BP in a dense-plasma environment. Combining the results of previous studies, we have proposed a single simple phenomenological expression for the fusion rate, valid in all five fusion regimes (which can be realized in the different $\rho - T$ regions). Our formula contains adjustable parameters whose variations reflect theoretical uncertainties of the reaction rates.

For illustration, we have considered (Sec. IV) the efficiency of carbon burning in dense matter and the conditions for carbon ignition in white dwarf cores and neutron star crusts. We show that carbon burning is actually important in a sufficiently narrow $\rho - T$ strip that is mainly determined by the temperature $T \sim (4 - 15) \times 10^8$ K as long as $\rho \lesssim 3 \times 10^9$ g cm^{-3}, and by the density $\rho \sim (3 - 50) \times 10^9$ g cm^{-3} as long as $T \lesssim 10^8$ K. On the basis of these results, we suggest that the current knowledge of nuclear fusion is sufficient for understanding the main features of carbon burning in stellar matter, especially at $\rho \lesssim 3 \times 10^9$ g cm^{-3}.

We have focused on the simplest case of heavy-ion burning in a one-component Coulomb system, particularly in a perfect crystal. There is no doubt that dense matter of white dwarfs and neutron stars are more complicated and require a more complex approach taking into account mixtures of different heavy nuclei and imperfections in dense matter. The complexity ranges from essentially two-component plasma conditions anticipated in the carbon oxygen cores of white dwarfs to the multicomponent isotope distribution in the ashes of accreting neutron stars [67].

In a forthcoming paper we will expand the presented analysis to the case of the fusion rates between different isotopes. We will employ this formalism for calculating the *S* factors for a broad range of heavy-ion fusion reactions. We will include the results in a pycno-thermonuclear reaction network and simulate the nucleosynthesis in high-density stellar matter.

[1] G. Wallerstein *et al.*, Rev. Mod. Phys. **69**, 995 (1997).

[2] C. A. Barnes, S. Trentalange, and S.-C. Wu, in *Treatise on Heavy-Ion Science* edited by D. A. Bromley (Plenum, New York, 1985), Vol. 6, p.3.

[3] T. A. Weaver and S. E. Woosley, Phys. Rep. **227**, 65 (1993).

[4] S. E. Woosley, Alexander Heger, T. Rauscher, and R. D. Hoffman, Nucl. Phys. **A718**, 3 (2003).

[5] W. Hillebrandt and J. C. Niemeyer, Annu. Rev. Astron. Astrophys. **38**, 191 (2000).

[6] S. E. Woosley, S. Wunsch, and M. Kuhlen, Astrophys. J. **607**, 921 (2004).

[7] I. Baraffe, A. Heger, and S. E. Woosley, Astrophys. J. **615**, L378 (2004).

[8] E. E. Salpeter, Aust. J. Phys. **7**, 373 (1954).

[9] R. Cussons, K. Langanke, and T. Liolios, Eur. Phys. J. A **15**, 291 (2002).

[10] A. Cumming and L. Bildsten, Astrophys. J. Lett. **559**, L127 (2001).

[11] T. E. Strohmayer and E. F. Brown, Astrophys. J. **566**, 1045 (2002).

[12] R. L. Cooper and R. Narayan, Astrophys. J., (to be published).

[13] H. Schatz, L. Bildsten, and A. Cumming, Astrophys. J. Lett. **583**, L87 (2003).

[14] P. Haensel and J. L. Zdunik, Astron. Astrophys. **229**, 117 (1990); **404**, L33 (2003) .

[15] E. E. Salpeter and H. M. Van Horn, Astrophys. J. **155**, 183 (1969).

[16] S. Schramm and S. E. Koonin, Astrophys. J. **365**, 296 (1990); **377**, 343(E) (1991).

[17] M. A. Cândido Ribeiro, L. C. Chamon, D. Pereira, M. S. Hussein, and D. Galetti, Phys. Rev. Lett. **78**, 3270 (1997).

[18] L. C. Chamon, D. Pereira, M. S. Hussein, M. A. Cândido Ribeiro, and D. Galetti, Phys. Rev. Lett. **79**, 5218 (1997).

[19] L. C. Chamon, D. Pereira, and M. S. Hussein, Phys. Rev. C **58**, 576 (1998).

[20] L. C. Chamon, B. V. Carlson, L. R. Gasques, D. Pereira, C. De Conti, M. A. G. Alvarez, M. S. Hussein, M. A. Candido Ribeiro, E. S. Rossi, Jr., and C. P. Silva, Phys. Rev. C **66**, 014610 (2002).

[21] L. R. Gasques, L. C. Chamon, D. Pereira, M. A. G. Alvarez, E. S. Rossi, Jr., C. P. Silva, and B. V. Carlson, Phys. Rev. C **69**, 034603 (2004), and references therein.

[22] A. V. Afanasjev, P. Ring, and J. König, Nucl. Phys. **A676**, 196 (2000).

[23] A. V. Afanasjev, J. König, and P. Ring, Phys. Rev. C **60**, 051303(R) (1999).

[24] T. Gonzalez-Llarena, J. L. Edigo, G. A. Lalazissis, and P. Ring, Phys. Lett. **B379**, 13 (1996).

[25] P.-G. Reinhard, M. Rufa, J. Maruhn, W. Greiner, and J. Friedrich, Z. Phys. A **323**, 13 (1986).

[26] G. A. Lalazissis, J. König, and P. Ring, Phys. Rev. C **55**, 540 (1997).

[27] T. Nikšić, D. Vretenar, P. Finelli, and P. Ring, Phys. Rev. C **66**, 024306 (2002).

[28] G. A. Lalazissis, T. Nikšić, D. Vretenar, and P. Ring, Phys. Rev. C **71**, 024312 (2005).

[29] L. R. Gasques, L. C. Chamon, C. P. Silva, D. Pereira, M. A. G. Alvarez, E. S. Rossi, Jr., V. P. Likhachev, B. V. Carlson, and C. De Conti, Phys. Rev. C **65**, 044314 (2002).

[30] D. L. Hill and J. A. Wheeler, Phys. Rev. **89**, 1102 (1953).

[31] L. I. Schiff, *Quantum Mechanics*, International series in pure and applied physics, 3rd ed. (McGraw-Hill, New York, 1968).

[32] W. A. Fowler, G. R. Caughlan, and B. A. Zimmerman, Annu. Rev. Astron. Astrophys. **13**, 69 (1975).

[33] J. R. Patterson, H. Winkler, and C. S. Zaidins, Astrophys. J. **157**, 367 (1969).

[34] M. G. Mazarakis and W. E. Stephens, Phys. Rev. C **7**, 1280 (1973).

[35] M. D. High and B. Cujec, Nucl. Phys. **A282**, 181 (1977).

[36] P. Rosales *et al.*, Rev. Mex. Fís. **49**, Suppl. 4, 88 (2003).

[37] K. U. Kettner, H. Lorenz-Wirzba, and C. Rolfs, Z. Phys. A **298**, 65 (1980).

[38] H. W. Becker *et al.*, Z. Phys. A **303**, 305 (1981).

[39] S. Ohkubo and D. M. Brink, Phys. Rev. C **36**, 966 (1987).

[40] G. J. Michaud and E. W. Vogt, Phys. Rev. C **5**, 350 (1972).

[41] W. Treu, H. Fröhlich, W. Galster, P. Dück, and H. Voit, Phys. Rev. C **22**, 2462 (1980).

[42] M. A. G. Alvarez *et al.*, Nucl. Phys. **A723**, 93 (2003).

[43] H. E. DeWitt, W. Slattery, D. Baiko, and D. Yakovlev, Contrib. Plasma Phys. **41**, 251 (2001).

[44] A. Alastuey and B. Jancovici, Astrophys. J. **226**, 1034 (1978).

[45] S. Ogata, Astrophys. J. **481**, 883 (1997).

[46] D. G. Yakovlev and D. A. Shalybkov, Sov. Sci. Rev. Sec. E **7**, 313 (1989).

[47] H. E. DeWitt, H. C. Graboske, and M. S. Cooper, Astrophys. J. **181**, 439 (1973).

[48] Y. Rosenfeld, Phys. Rev. E **53**, 2000 (1996).

[49] B. Jancovici, J. Stat. Phys. **17**, 357 (1977).

[50] H. DeWitt and W. Slattery, Contrib. Plasma Phys. **43**, 279 (2003).

[51] A. Y. Potekhin and G. Chabrier, Phys. Rev. E **62**, 8554 (2000).

[52] H. DeWitt and W. Slattery, Contrib. Plasma Phys. **39**, 97 (1999).

[53] S. Ogata, H. Iyetomi, and S. Ichimaru, Astrophys. J. **372**, 259 (1991)

[54] S. Ogata, S. Ichimaru, and H. M. Van Horn, Astrophys. J. **417**, 265 (1993).

[55] E. L. Pollock and B. Militzer, Phys. Rev. Lett. **92**, 021101 (2004).

[56] S. L. Shapiro and S. A. Teukolsky, *Black Holes, White Dwarfs, and Neutron Stars* (Wiley-Interscience, New York, 1983).

[57] D. A. Baiko, Phys. Rev. E **66**, 056405 (2002).

[58] S. Ichimaru, S. Ogata, and H. M. Van Horn, Astrophys. J. **401**, L35 (1992).

[59] H. Kitamura and S. Ichimaru, Astrophys. J. **438**, 300 (1995).

[60] D. A. Baiko, A. D. Kaminker, A. Y. Potekhin, and D. G. Yakovlev, Phys. Rev. Lett. **81**, 5556 (1998).

[61] S. Ichimaru and H. Kitamura, Phys. Plasmas **6**, 2649 (1999); Erratum: **7**, 1335 (2000).

[62] H. Kitamura, Astrophys. J. **539**, 888 (2000).

[63] A. V. Filippenko, in *White Dwarfs: Probes of Galactic Structure and Cosmology*, edited by E. M. Sion, H. L. Shipman, and S. Vennes (Kluwer, Dordrecht, The Netherlands, in press).

[64] N. Itoh, H. Mutoh, A. Hikita, and Y. Kohyama, Astrophys. J. **395**, 622 (1992); Erratum: **404**, 418 (1993).

[65] A. D. Kaminker, C. J. Pethick, A. Y. Potekhin, V. Thorsson, and D. G. Yakovlev, Astron. Astrophys. **343**, 1009 (1999).

[66] M. E. Raikh and D. G. Yakovlev, Astrophys. Space Sci. **87**, 193 (1982).

[67] S. E. Woosley, A. Heger, A. Cumming, R. D. Hoffman, J. Pruet, T. Rauscher, J. L. Fisker, H Schatz, B. A. Brown, and M. Wiescher, Astrophys. J. Suppl. **151**, 75 (2004).